Article

Low-Temperature Fluorocarbonate Mineralization in Lower Devonian Rhynie Chert, UK

John Parnell [1,*]**, Temitope O. Akinsanpe** [1,2]**, John W. Still** [1]**, Andrea Schito** [1]**, Stephen A. Bowden** [1]**, David K. Muirhead** [1] **and Joseph G. T. Armstrong** [1]

---

[1] School of Geosciences, University of Aberdeen, King's College, Aberdeen AB24 3UE, UK; t.akinsanpe.18@abdn.ac.uk (T.O.A.); j.still@abdn.ac.uk (J.W.S.); andrea.schito@abdn.ac.uk (A.S.); s.a.bowden@abdn.ac.uk (S.A.B.); dmuirhead@abdn.ac.uk (D.K.M.); joseph.armstrong@abdn.ac.uk (J.G.T.A.)
[2] Department of Geology, Obafemi Awolowo University, Ile-Ife 220103, Nigeria
* Correspondence: j.parnell@abdn.ac.uk

Abstract: Rare earth element (REE) fluorocarbonate mineralization occurs in lacustrine shales in the Lower Devonian Rhynie chert, Aberdeenshire, UK, preserved by hot spring silicification. Mineralization follows a combination of first-cycle erosion of granite to yield detrital monazite grains, bioweathering of the monazite to liberate REEs, and interaction with fluorine-rich hot spring fluids in an alkaline sedimentary environment. The mineral composition of most of the fluorocarbonates is referable to synchysite. Mineralization occurs at the surface, and the host shales subsequently experience maximum temperatures of about 110 °C. Most fluorocarbonate mineralization originates at much higher temperatures, but the Rhynie occurrence emphasizes that low-temperature deposits are possible when both fluorine and REEs are available from granite into the sedimentary environment.

Keywords: rare earth elements; synchysite; Rhynie chert; Scotland; hot spring

1. Introduction

Fluorocarbonates are the major source of rare earth elements [1–4]. It is, therefore, important that their origin is understood. The majority of known occurrences are associated with carbonatites and syenite intrusions [5–9], but they also form in high-temperature ore deposits [10–12]. However, there are also examples formed by relatively low-temperature processes, especially by the alteration of carbonatite [13] and granite [14]. This study reports an example in which a fluorocarbonate mineral was precipitated in shale following REE availability in surface conditions, in which biological action played a critical role.

The mineral occurrence is within the Lower Devonian Rhynie chert lagerstätte, which contains exceptionally preserved plants, fungi, and animals, and is considered to represent the world's oldest terrestrial ecosystem. The fossils occur in chert bed layers interbedded with sandstones and shales (Figures 1 and 2). Locally, the sandstones are interbedded with andesitic ash tuffs. The rocks are not exposed, but they are archived in a number of cores at the University of Aberdeen (Figure 3). Petrographic studies of the plant-bearing sediments show that detrital monazite grains exhibit extensive leaching. The alteration is attributable to fungi, whose remains are widespread in the deposit and which would have been pivotal to the supply of phosphorus for plant growth.

The Devonian continental sediments accumulated in a small basin bounded by an active normal fault, marked by a silicified breccia (Figure 1). The rocks are gently folded in the vicinity of the chert outcrop (Figure 1).

The sediments lie unconformably on Neoproterozoic metasediments of the Dalradian supergroup and Caledonian intrusions, including Ordovician 'Newer Gabbros' and Silurian–early Devonian granites (Figure 1). All of these basement rocks supplied detrital sediment to the Devonian, but immediately adjacent granite was a particularly likely source [15]. The detritus included REE-bearing monazite, which occurs in the local granite.
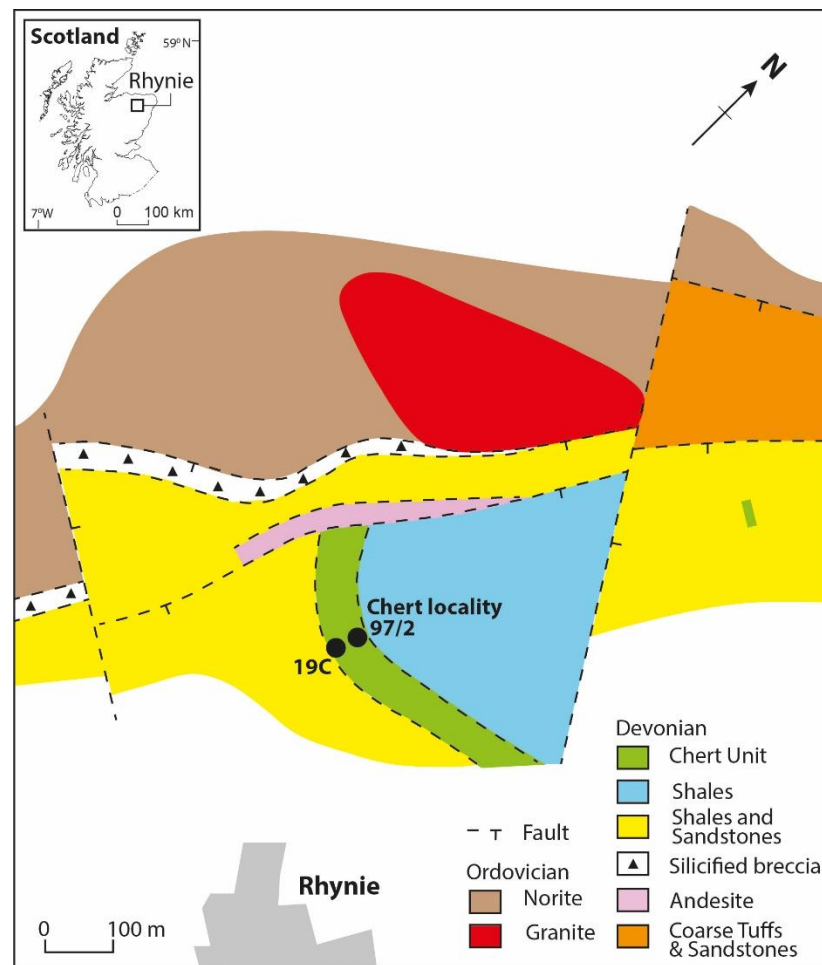
Figure 1. Geological map of region near Rhynie village, modified from [16]. Fluorocarbonate mineralization sampled from two boreholes (19C, 97/2) at Rhynie chert locality.
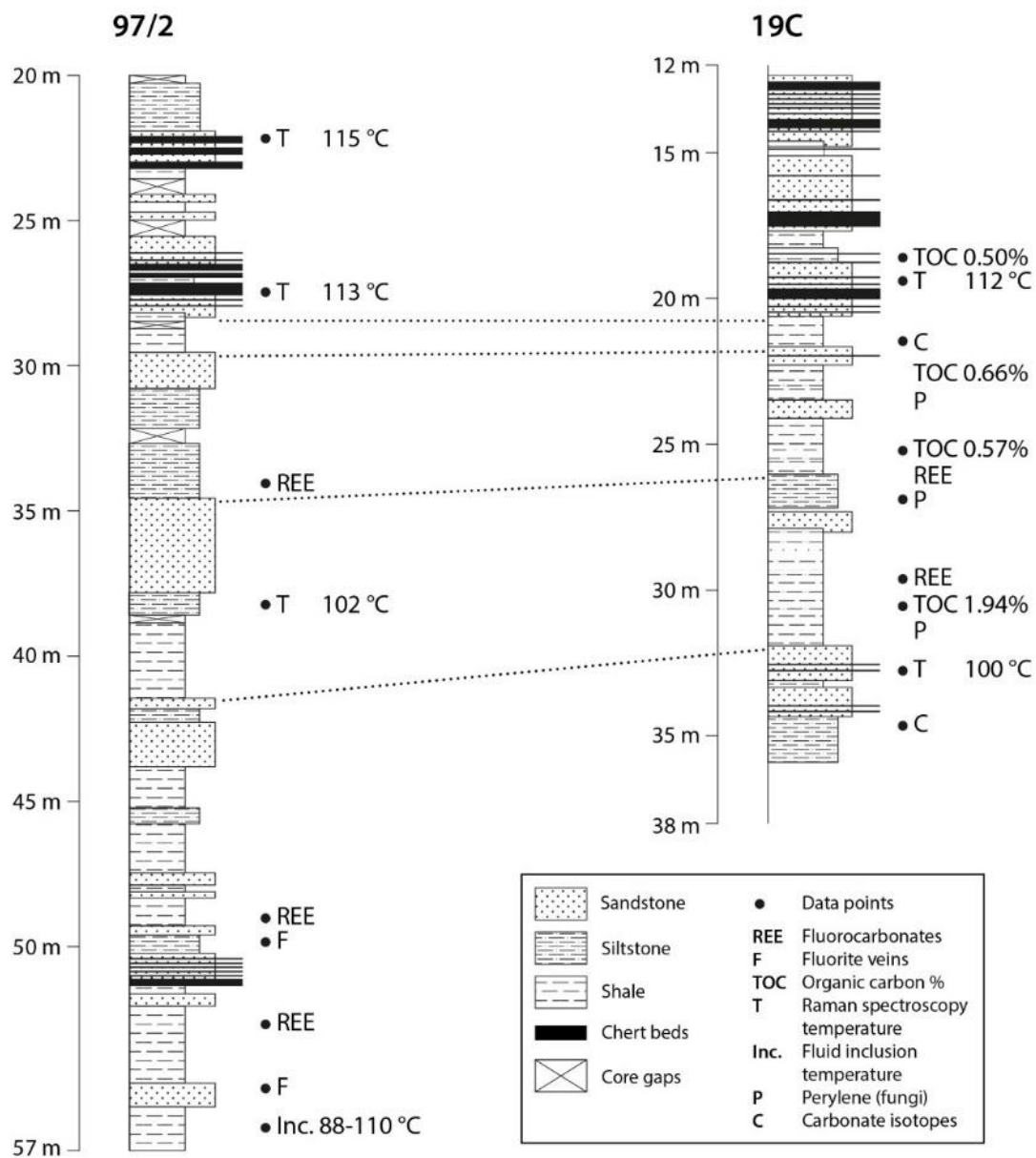
Figure 2. Lithological sections for portions of borehole cores 19C and 97/2, showing correlation horizons (after [17]), positions of fluorite veining [16], sampling for fluorocarbonate analysis (this study), TOC measurement (this study), Raman spectroscopy (this study), detection of perylene (this study), fluid inclusion analysis [18], and carbonate isotope analysis [15].

Monazite grains in sandstone beds below the Rhynie chert are rounded and unaltered, as is generally the case in sediments with a low-temperature history. Monazite in the granite is also unaltered. However, monazite grains in the chert-bearing succession are instead strongly altered to form a porous texture (Figure 4). The host sediment for the altered monazite contains abundant evidence of fungi [19–21], which are an expected cause of the alteration. Monazite grains exposed to fungi, either naturally or experimentally, exhibit extensive bioweathering [22–27]. Monazite is a source of phosphorus, which fungi release for uptake by plants as part of the fungus–plant symbiosis. In the process, REEs are also liberated from the monazite. An authigenic REE mineral phase recorded here in the Rhynie succession may, therefore, represent the REEs released from the Rhynie monazite. The REE phase occurs in shales which are interpreted as lacustrine deposits, interbedded with fluvial sediments that contain the plant fossils for which the Rhynie chert is internationally important [28].
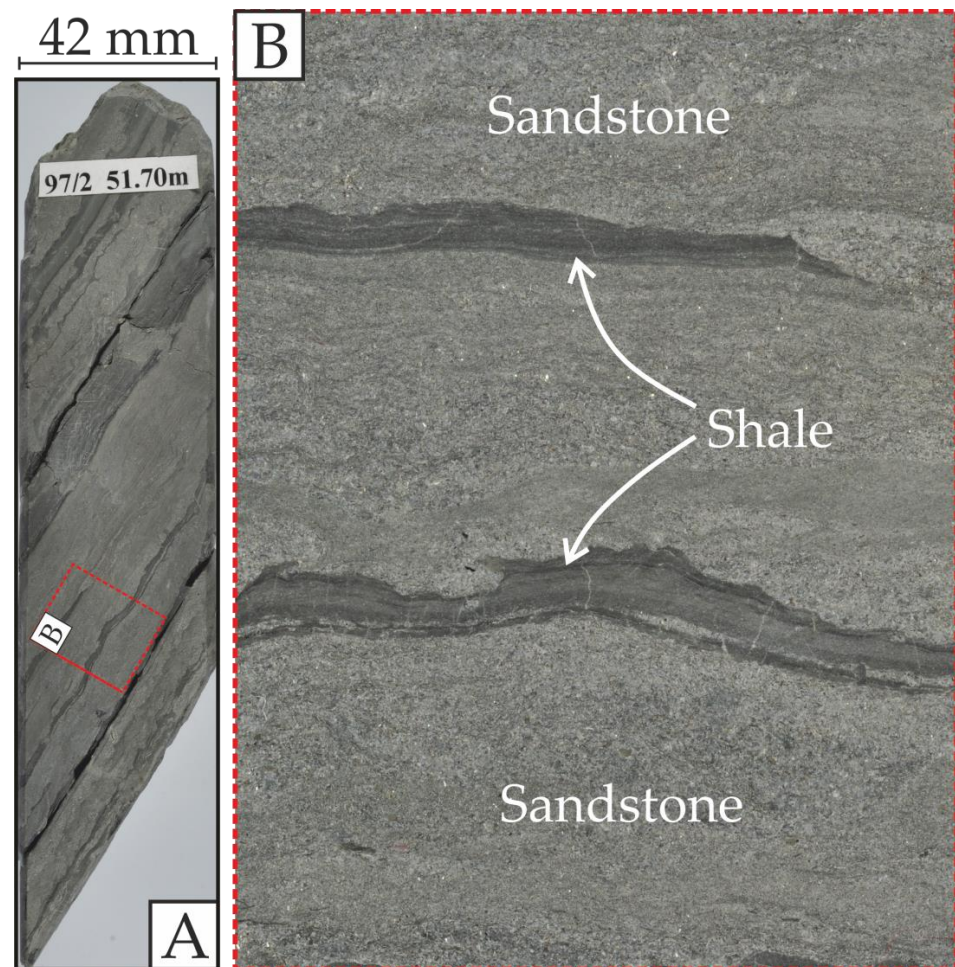
Figure 3. Portion of core (width 42 mm) through sandstone and shale from borehole 97/2, at depth where fluorite and fluorocarbonate mineralization occur in shales. (**A**) full core, width 42 mm; (**B**) detail of core.
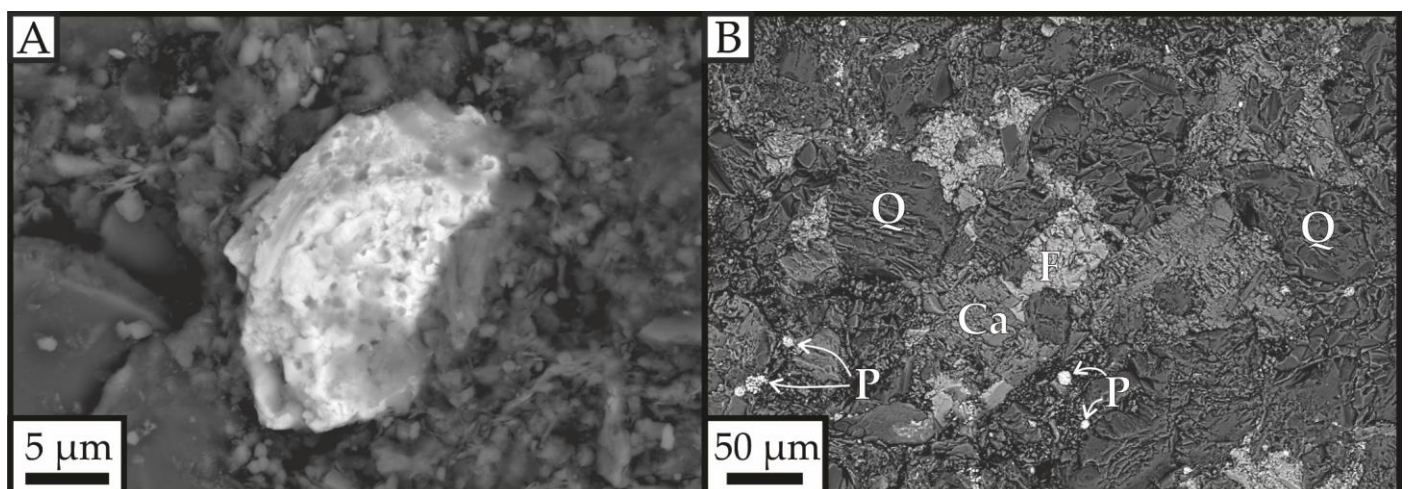
Figure 4. Backscattered electron micrographs of mineralogy in rocks hosting fluorocarbonate mineralization. (**A**) weathered monazite grain, borehole 19C, depth 26.5 m; (**B**) shale cemented by fluorite (light grey) and calcite (dark grey), with pyrite framboids (bright), borehole 97/2, depth 50.2 m. Ca, calcite; F, fluorite; P, pyrite; Q, detrital quartz.

The REE phase is characterized here by:

(i) Measurement of the chemical composition of the mineral.
(ii) Comparison with the composition of known fluorocarbonate mineralization and identification of the phase.
(iii) Constraints on the temperature of formation.

2. Materials and Methods

Shale and sandstone samples were taken from cores 97/2 (Figure 3) and 19C, in the immediate vicinity of the plant-bearing chert outcrop (Figures 1 and 2). The stratigraphy of the cores and the correlation between them (Figure 2) are described in [26]. The cores were drilled to help delineate the extent of the plant-bearing deposits [17,28].

Petrographic studies were performed at the University of Aberdeen ACEMAC Facility using a Carl Zeiss Gemini 300 VP field emission gun scanning electron microscope (FEG-SEM) on polished blocks of rock. Samples were carbon-coated and analysed at 20 kV with a working distance of 10.5 mm. Samples were analysed using an Oxford Instruments NanoAnalysis Xmax80 Energy Dispersive Spectroscopy (EDS) detector and the AZtec software suite. For routine work, the beam diameter is just a few nanometres, but the X-ray excitation volume is larger than the beam diameter. Spectra were recorded using a live time of either 18 s or 25 s. The standards used were a mixture of natural minerals, metal oxides, and pure metals, as calibrated by the factory. The element weight percent detection limits relevant to this study are 0.28% F, 0.27% Y, 0.32% Gd, and 0.38%–0.44% for other REEs. Carbonate contents were determined by stoichiometry. The compositions of fluorocarbonate grains (Table 1) were identified by comparison with mean compositions for phases interpreted as synchysite and parisite in published case studies (Table 2).

Fungal activity in the succession was tested using the detection of the biomarker perylene, which records such activity in the geological record [29]. Gas chromatography–mass spectrometry was used to measure the mass fragment m/z 252, which records perylene.

The maximum temperature experienced by the host rock was derived from the thermal maturity of organic matter in shale and fine sandstone (Figure 2), determined by Raman spectroscopy. A Renishaw inVia reflex Raman spectrometer was used, with a backscattering geometry in the range of 700–3200 cm^{-1}, a 2400 L/mm spectrometer grating, and a CCD detector. Microscopic observations were carried out with a ×50 confocal optical power objective with a numerical aperture (NA) of 0.90. The slit opening was 65 um with a CCD area of approximately 10 pixels (80% of the total signal height hitting the CCD chip) and a confocal hole of 200 μm. A 514.5 nm diode laser was used for excitation with an output of 50 mW. Optical filters (1%) were used to adjust the power of the laser to less than 0.5 mW to avoid alteration [30]. Vitrinite reflectance equivalent values (Ro$_{eq}$%) were calculated from Raman spectra by using an approach [31] based on an automatic deconvolution in which D and G bands are fitted separately, applying a one-band asymmetrical Gaussian band fitting for each spectral region. Position, intensity, width, and integrated area of the D and G bands were determined and used to calculate Ro$_{eq}$% by means of a multi-parametric equation (see [31] for more details). Temperatures were calculated by converting vitrinite reflectance equivalent (Ro$_{eq}$%) by using the Barker and Pawlewicz equation [32].

Table 1. Selected analyses of fluorocarbonate minerals in borehole 97/2.

Oxide %	97/2 34.3 m					97/2 49.5 m		97/2 49.5 m			97/2 49.5 m	
	Site 11-1	Site 11-2	Site 11-3	Site 11-4	Site 11-7	Site 9-2	Site 9-7	Site 22-1	Site 22-4	Site 22-6	Site 25-1	Site 25-2
CaO	16.25	12.33	15.73	15.85	15.99	14.50	14.45	14.76	12.69	15.29	15.42	16.39
La_2O_3	13.23	14.57	12.88	13.73	13.43	11.34	12.24	15.42	12.67	11.76	11.06	11.19
Ce_2O_3	24.97	26.32	24.27	25.85	26.71	23.55	23.93	25.18	24.51	22.73	24.16	23.68
Pr_2O_3	2.72	2.20	2.46	2.94	2.94	2.70	2.53	2.50	2.73	2.54	2.96	2.48
Nd_2O_3	9.23	9.61	8.99	9.62	10.25	10.18	9.86	8.04	10.22	9.13	9.76	10.11
Sm_2O_3	1.33	1.18	1.40	1.42	1.76	1.72	1.46	1.51	1.25	1.54	1.76	1.87
Gd_2O_3	0.68	0.00	0.00	0.66	0.69	0.80	0.80	1.01	0.84	0.89	1.18	0.99
Y_2O_3	0.00	0.00	0.33	0.00	0.00	0.37	0.00	0.72	0.50	0.56	0.91	0.95
CO_2	29.72	23.00	29.49	29.64	29.99	26.89	28.11	29.92	25.75	29.45	28.04	27.73
F	3.36	7.13	2.65	3.88	4.20	4.13	3.06	3.08	4.64	1.98	4.24	4.99
Total	101.48	96.34	98.20	103.59	105.96	96.18	96.43	102.15	95.79	95.89	99.50	100.38
$-O \equiv F$	1.41	3.00	1.12	1.63	1.77	1.74	1.29	1.30	1.95	0.83	1.79	2.10
TOTAL	100.07	93.34	97.08	101.95	104.19	94.44	95.15	100.85	93.84	95.05	97.71	98.27
Elemental %												
Ca	0.92	0.79	0.91	0.89	0.88	0.88	0.87	0.84	0.79	0.90	0.90	0.95
La	0.26	0.32	0.26	0.27	0.26	0.24	0.25	0.30	0.27	0.24	0.22	0.22
Ce	0.48	0.58	0.48	0.50	0.50	0.49	0.49	0.49	0.52	0.46	0.48	0.47
Pr	0.05	0.05	0.05	0.06	0.06	0.06	0.05	0.05	0.06	0.05	0.06	0.05
Nd	0.17	0.21	0.17	0.18	0.19	0.21	0.20	0.15	0.21	0.18	0.19	0.20
Sm	0.02	0.02	0.03	0.03	0.03	0.03	0.03	0.03	0.03	0.03	0.03	0.04
Gd	0.01	0.00	0.00	0.01	0.01	0.01	0.01	0.02	0.02	0.02	0.02	0.02
Y	0.00	0.00	0.01	0.00	0.00	0.01	0.00	0.02	0.02	0.02	0.03	0.03
REE total	1.00	1.18	1.00	1.03	1.04	1.05	1.04	1.05	1.12	0.99	1.04	1.02
C	2.15	1.88	2.18	2.12	2.11	2.09	2.15	2.16	2.05	2.22	2.09	2.05
F	0.56	1.35	0.45	0.64	0.68	0.74	0.54	0.52	0.86	0.35	0.73	0.85
F/Ca	0.61	1.71	0.50	0.72	0.78	0.84	0.62	0.62	1.08	0.38	0.81	0.90
REE/Ca	1.09	1.49	1.09	1.16	1.19	1.19	1.19	1.26	1.42	1.10	1.15	1.07
Identity	synchysite	Intermed. synchysite-parisite	synchysite	synchysite	synchysite	synchysite	synchysite	synchysite	Intermed. synchysite-parisite	synchysite	synchysite	synchysite

Table 2. Examples of settings for fluorocarbonate mineralization, and mean values of atomic ratios for synchysite and parisite.

Mineral	Location	Setting	Mineralization Temperature	Mean F/Ca (atomic)	Mean REE/Ca (atomic)	Reference
Synchysite	NE Vietnam	Hydrothermal base metal	~400 °C	0.50	0.97	[10]
Synchysite	Olympic Dam, Australia	Breccia-hosted iron oxide	~300 °C	0.55	1.00	[11]
Synchysite	South Hungary	Coal, intruded	<200 °C	0.57	0.98	[33]
Synchysite	Cinquevalli, Italy	Ag-Cu-quartz veins		0.58	1.01	[34]
Synchysite	Rif, Morocco	Pelites	420–450 °C	0.71	1.06	[35]
Synchysite	Anti-Atlas, Morocco	Syenite	>150–250 °C	0.71	0.94	[5]
Synchysite	Erzgebirge, Germany	Altered granite	550–600 °C	0.80	1.13	[36]
Synchysite	Rozna, Czech Republic	U deposit	<100 °C	0.84	0.86	[37]
Synchysite	Jiangxi, China	Weathered granite	<100 °C	0.87	0.99	[14]
Parisite	Parana Basin, Brazil	Carbonatite	<375 °C	1.02	1.30	[6]
Parisite	Gujarat, India	Altered Carbonatite	100–150 °C	1.22	2.21	[13]
Parisite	Bergslagen, Sweden	Metavolcanics, iron oxide ore	>400 °C	1.32	2.05	[12]
Parisite	Eastern Tibet	Carbonatite-syenite	200–300 °C	1.44		[7]
Parisite	Qinling, China	Carbonatite	<265 °C	1.46	2.05	[38]
Parisite	South Urals, Russia	Volcanic massive sulfide	80–300 °C	1.51	1.80	[39]
Parisite	Wyoming, USA	Carbonatite	<250 °C	1.70	2.09	[8]
Parisite	Aar Massif, Switzerland	Granite, hydrothermal	~300 °C	1.87	1.63	[40]
Parisite	Thor Lake, Canada	Syenite	<600 °C	1.95	2.23	[9]
Parisite	Maripí, Colombia	Emeralds in black shale	290–360 °C	1.97	2.02	[41]
Fluoro-carbonate	Rhynie Chert	Black shale	100–115 °C	0.85	1.10	This study

3. Results

The lacustrine sediments consist of millimetre-to-centimetre scale beds of black shale (mudstone, siltstone) with interbedded streaks of fine sandstone. The sandstone is calcite-cemented and additionally may have sub-millimetre laminae of pure carbonate. At about a 50 m depth in borehole 97/2, sandstone is also cemented by fluorite (Figure 4). The shales consist of detrital quartz, feldspar, micas, chloritoid grains, and fragments of organic plant matter. The organic matter is concentrated in specific layers. Accessory minerals include zircon, garnet, monazite, and xenotime. Among these grains are framboids and solid crystals of pyrite, as well as crystals of REE–fluorocarbonate. The pyrite framboids are mostly 20 microns in diameter or smaller, and they include traces of arsenic and/or manganese. The REE–fluorocarbonate is typically 3 to 10 microns in size and forms irregular shapes in a matrix of microquartz crystals and clay (Figure 5). The small size of the crystals means they are of mineralogical interest only and do not represent an anomalous REE concentration.
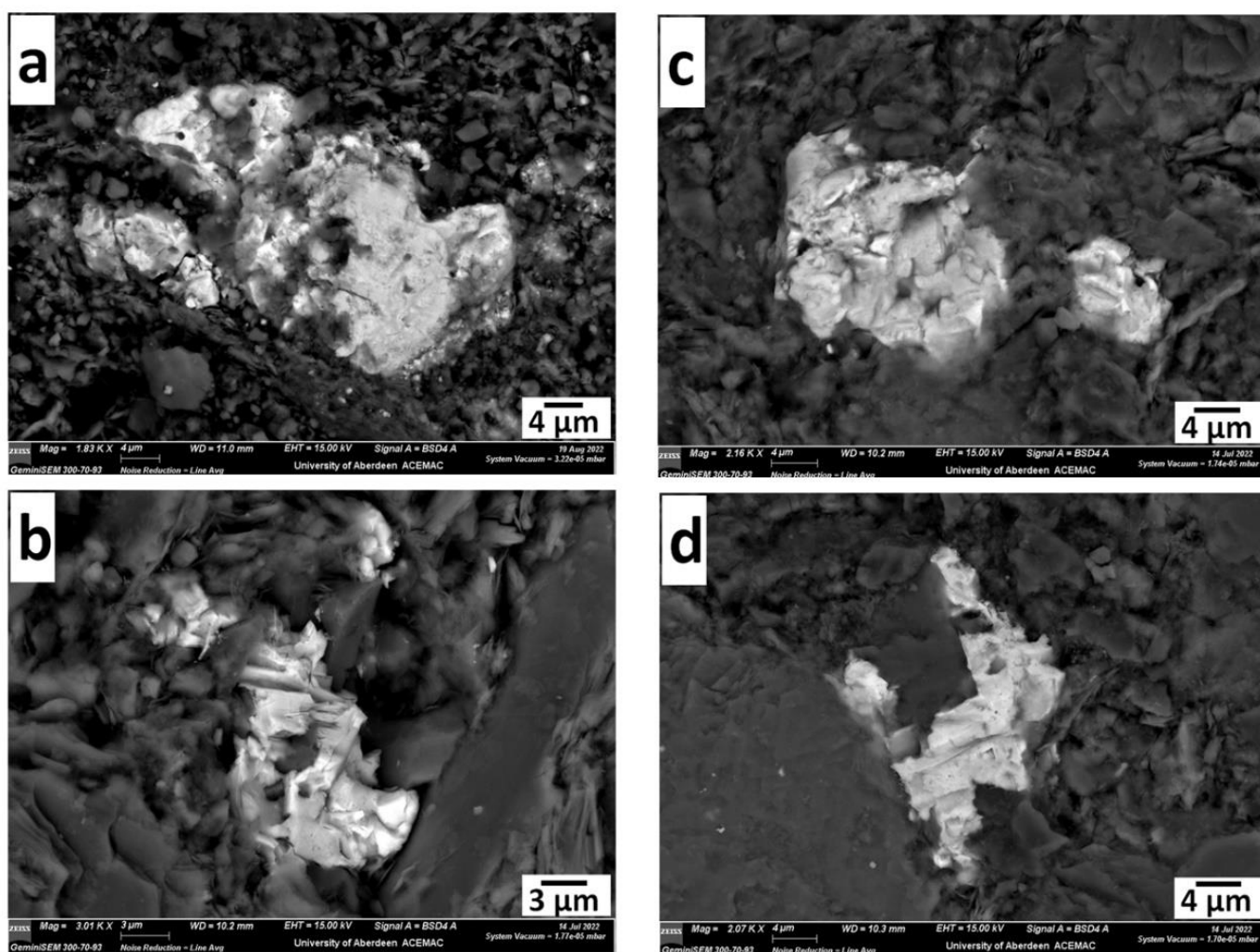
Figure 5. Backscattered electron micrographs of fluorocarbonate mineralization, Rhynie chert succession. Fluorocarbonate crystals (bright) in microquartz/clay matrix show a delicate form typical of diagenetic growth. (**a**) borehole 19C, depth 26.5 m; (**b**–**d**) borehole 97/2 depth 49.5 m.

Samples containing fluorocarbonate mineralization are located in both cores 19C and 97/2 (Figure 2). Mineralization was found in five samples, covering a 20 m depth range in core 97/2 (Figure 2). In the immediate vicinity, several shale samples in the sections

(Figure 2) contain at least 0.5% total organic carbon (TOC) and thus can be classified as black shales [42,43].

The majority of the 41 compositions measured in the Rhynie fluorocarbonates (12 highest totals and lowest contaminations from Si in surrounding silicate are shown in Table 1) are similar to mean published compositions for synchysite (Figure 6). There are, however, several compositions measured at Rhynie that either plot with published parisite data or have intermediate compositions (Figure 6). The synchysite is cerium-rich (20–25 wt. % Ce_2O_3), with lower lanthanum (10–15 wt. % La_2O_3) and neodymium (8–10 wt. % Nd_2O_3), and minor contents of yttrium and other REEs (Table 1). Minor deviations from 100% totals are due to contamination from surrounding silicate and variable substitution by the -OH anion.
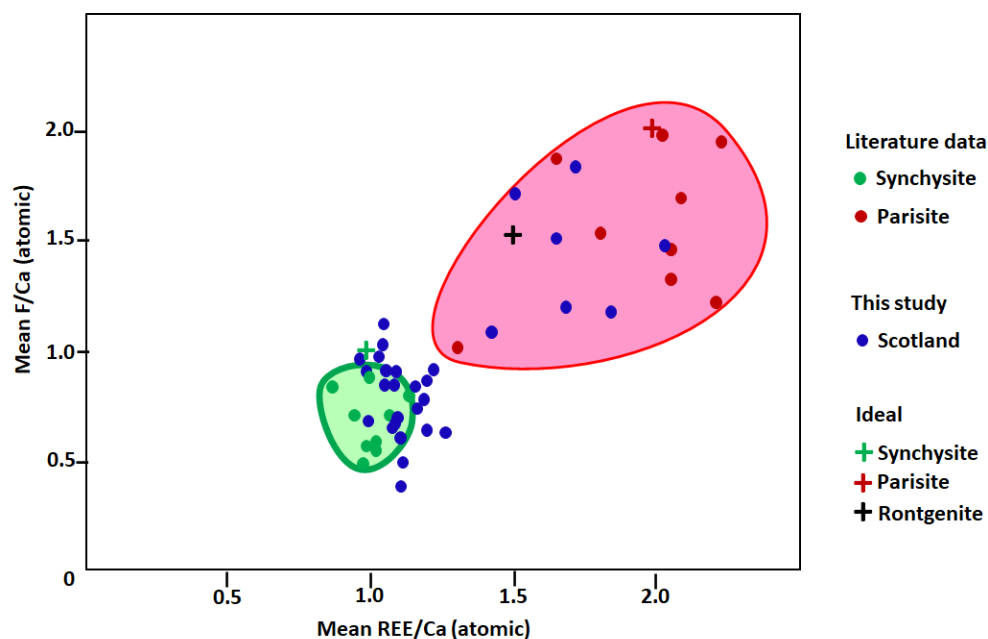
Figure 6. Cross-plot of mean atomic ratios for REE/Ca and F/Ca in fluorocarbonate minerals synchysite and parisite reported in the literature (Table 2), also showing compositions measured in the Rhynie chert, which are predominantly in the synchysite field. The ideal compositions for fluorocarbonate mineral species are shown.

Three samples of shale analysed by GC-MS record the distinctive peak of perylene in mass fragment 252 (Figures 2 and 7). Perylene is an aromatic cyclic hydrocarbon with the formula $C_{20}H_{12}$.

Analyses of carbonaceous matter by Raman spectroscopy were performed on thin-section samples of shale and fine sandstone (Figure 2). Up to sixteen spectra were acquired in each sample depending on the abundance of carbonaceous matter. Organic matter spectra exhibit both ordered and disordered peaks (i.e., D and G bands), superimposed on a fluorescence background. Ro_{eq}% values vary between 0.66% and 0.73%, indicating the mature stage of hydrocarbon generation (oil window). Associated maximum paleotemperatures, calculated by the conversion of Ro_{eq}% values [32], range between 100 and 115 °C (Table 3).
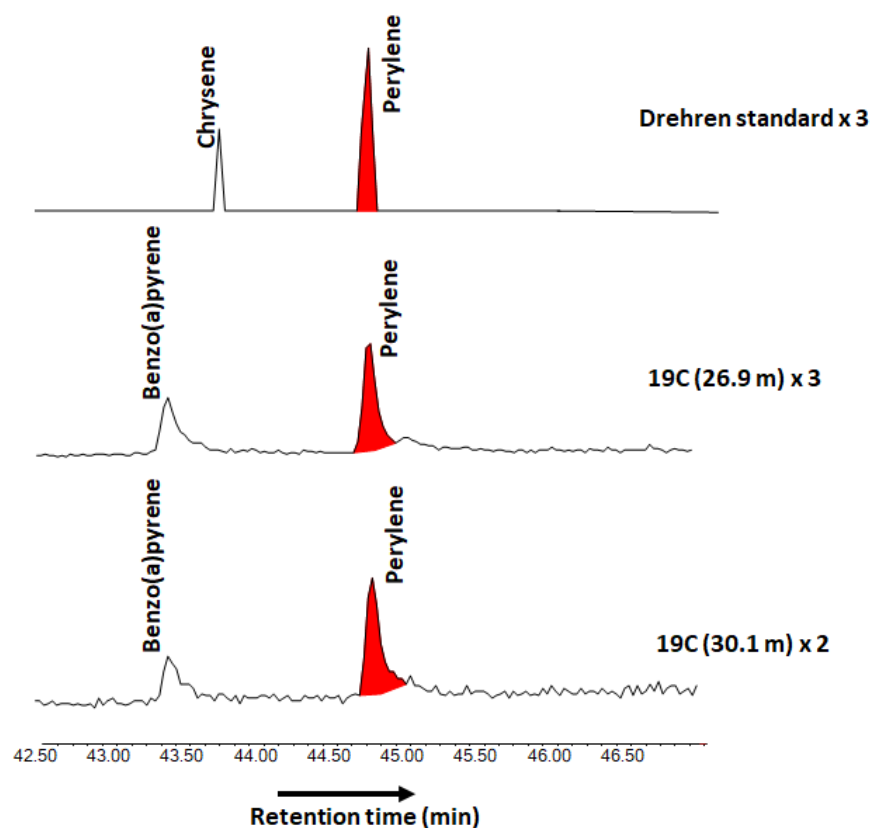
Figure 7. Mass spectra (m/z 252) for two samples of shale from core 19C, showing distinctive peak for perylene (red), indicating fungal activity. Peak identified using Drehren standard (Dr. Ehrenstorfer deuterated internal standard).

Table 3. Vitrinite reflectance equivalent and maximum temperatures for five samples from Rhynie boreholes. Temperatures were calculated according to the conversion of $Ro_{eq}\%$ values using equation [32]. sd, standard deviation.

Borehole	Depth (m)	$Ro_{eq}\%$	sd	Temperature (°C)	sd	*n*
	30.00	0.73	0.11	112.8	18.9	16
97/2	22.30	0.74	0.10	114.7	17.7	7
	38.50	0.67	0.05	102.4	9.8	10
19C	19.60	0.73	0.11	112.1	20.7	10
	33.55	0.66	0.06	100.4	10.8	3

4. Discussion

4.1. Requirements for Fluorocarbonate Mineralization

The irregular shape of the fluorocarbonate indicates that it is in a diagenetic phase, and fluorocarbonate minerals in sedimentary rocks are considered to be authigenic rather than detrital grains [44]. The crystal size is comparable with many published examples. Growth during diagenesis is consistent with the deposition of fluorite cement in the interbedded sandstones. The accompanying diagenetic mineralogy of pyrite framboids and calcite implies that the environment was anoxic and alkaline [45]. These characteristics help to show how fluorocarbonate mineralization occurred at Rhynie.

Fluorocarbonate minerals occur in a diversity of settings (Table 2). They are most commonly found in carbonatites, especially carbonatites that have experienced hydrothermal alteration (e.g., [13,38]). Other settings include a range of hydrothermal systems, massive sulphides, laterites/bauxites, and black shales (Table 2). Occurrences in shales and pelites (e.g., [35,41]) are assumed to reflect a high content of trace elements, including

REEs, in the depositional environment, promoted by the low-Eh conditions conferred by organic matter. The REEs were subsequently concentrated during diagenesis and metamorphism. In the case of Rhynie, REEs released during monazite alteration would have entered groundwaters and become fixed by organic matter in the sediment.

The hot springs that caused the Rhynie chert deposit to be preserved by silicification were also the source of the fluorine that contributed to the fluorocarbonate mineralization. Many hot springs contain anonymously high fluorine contents, and they may consequently be a cause of dental problems if the water enters the drinking supply [46–48]. Fluorine in the Rhynie hot spring system is evidenced by fluorite–calcite veins cutting the lower part of the chert succession [16,18]. Shales and fine sandstones also show mixed fluorite and calcite cement (Figure 4), showing that fluorine was able to enter the sediment matrix and react with other components.

The precipitation of fluorocarbonates further required an alkaline environment, which is evidenced by the carbonate laminae and calcite cement. Limited stable isotope data for the carbonates (sampling points in Figure 2) implies an early diagenetic origin [15]. The combination of calcite, organic matter, and pyrite constrains the conditions of the peat-like environment [49] to a limited Eh–pH space (Figure 8) that is appropriate for fluorocarbonate deposition [50].
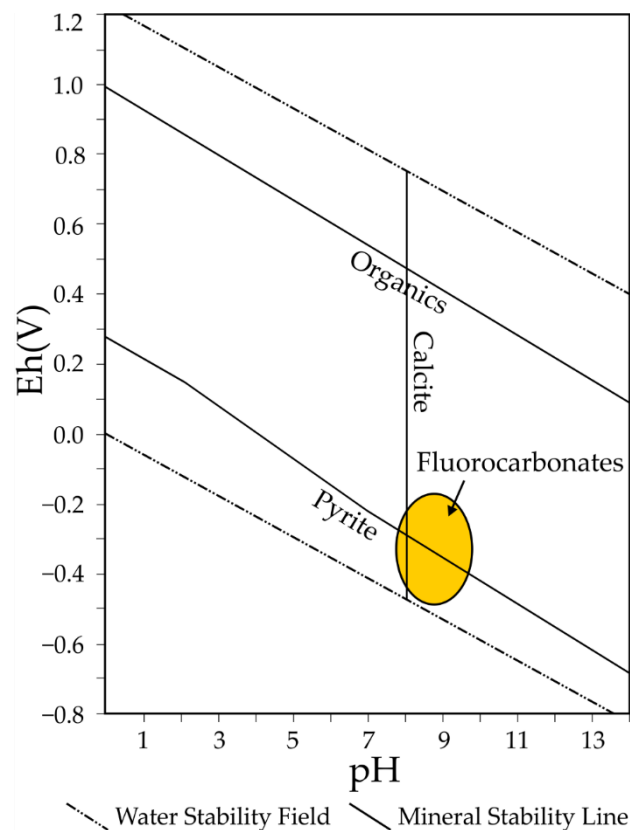
Figure 8. Pourbaix diagram for peatland environments, showing constraints imposed by the occurrence of organic matter, calcite, and pyrite (after [49]), and approximate conditions for fluorocarbonate mineral precipitation (after [50]).

4.2. Role of Granite

The fluorocarbonate mineralization is in sediments, but granite played a critical role. Firstly, the monazite grains that yielded the REEs during diagenesis were derived from underlying Caledonian granites. The attribution of monazite grains in the Devonian sediments to the granite was one of the earliest studies of provenance using heavy mineral analysis [51]. Secondly, the granites are enriched in fluorine [52,53], which caused fluorite mineralization in the Rhynie chert. High fluorine contents are indicated by high lithium

contents in the granite micas, as the two elements show positive covariance [54]. A regional input of fluorine-rich fluid is also evident in fluorite mineralization, which occurs where Dalradian Supergroup (late Neoproterozoic) limestones were intruded by Caledonian granites on Deeside, 30 km to the south [55,56]. The Ballater and Mount Battock granites on Deeside are both dated at 406 Ma [57], within error of the Rhynie chert dated at 407 Ma [58]. Another Caledonian granite in the vicinity contains fluorine-bearing zinnwaldite [59,60]. Further evidence of the role of the granites in mineralizing the Rhynie chert is in the precipitation of tungsten-bearing rutile in the chert [61], which reflects derivation from granites that are also mineralized by tungsten [60,62]. The fluorocarbonates at Rhynie are of mineralogical, rather than commercial, interest. However, the occurrence adds to the evidence for the flux of mineralizing fluids in the region, which could reflect as yet-undiscovered ore deposits.

4.3. Identification of Fluorocarbonate Mineral

The most widespread fluorocarbonate minerals in the Rhynie occurrence are synchysite $Ca(REE)(CO_3)_2F$ and parisite $Ca(REE)_2(CO_3)_3F_2$. In both synchysite and parisite, the F/Ca atomic ratios commonly fall below the ideal stoichiometric values, i.e., below 1 and 2, respectively. This is mostly a consequence of hydroxyl (-OH) substitution for fluoride (-F), which can occur up to several 10 s % (e.g., [5,34,41]). Thus, in several deposits, mean F/Ca ratios for synchysite are in the range of 0.5 to 0.6 [10,11,34]. The median value determined for the fluorocarbonate phase at Rhynie is 0.85 ($n = 41$), which is consistent with synchysite rather than parisite. Similarly, the median REE/Ca atomic ratio of the Rhynie phase is 1.10 ($n = 41$), which is comparable with values for other synchysite occurrences. The data that show a plot between synchysite and parisite indicate that some grains may not be synchysite. We omit the intermediate rontgenite (rongtenite, röngtenite), as it is not universally used (Figure 6). Other case studies report fine intermixtures of synchysite and parisite [6,13,38], which would explain the range of the Rhynie data. Synchysite occurs as Ce-, La-, Nd-, and Y-rich forms, and it is Ce-rich in this case. Many of the compositions may therefore be attributed to synchysite-(Ce) [34]. The profile of REEs (Ce > La > Nd >> others) is similar to many other occurrences of synchysite. It is also similar to the profile of REEs in typical monazite [63,64], which is consistent with a source for the fluorocarbonate REEs by the alteration of monazite. The apparent non-stoichiometry at the SEM scale is also explainable in terms of nanoscale disorder, or possibly unnamed phases [65,66]. There are also OH-dominant members of the series, e.g., hydroxylbastnäsite-(Ce), which would influence the stoichiometry if present.

4.4. Temperature of Mineralization

The range of settings for fluorocarbonate mineralization results in a range of temperatures for their formation. Most examples were probably deposited at temperatures above 100–200 °C (Table 2). However, there are also low-temperature occurrences (Table 2), which implies that REE availability is the critical factor.

The temperature of the silica-rich fluid that formed the Rhynie chert was probably no more than 50 °C [18], and bioweathering of the monazite would have occurred in these cool conditions. The fluorite–calcite veins record primary aqueous fluid inclusion temperatures of 88 to 110 °C in fluorite [18], but rapid heat dissipation around narrow veins would leave the sediments unperturbed by the minor hydrothermal activity. The maximum temperature of the rock, determined by Raman spectroscopy of carbonaceous matter, is about 110 °C (Table 3), but that is accounted for by post-mineralization heating due to burial, during the late Palaeozoic (Carboniferous–Permian) [67]. The palynological study of samples in core 97/2 is in agreement with Ro_{eq}% values calculated from Raman spectroscopic analyses and confirms that the organic matter has relatively low thermal maturity [68].

4.5. Biological Contribution to REE Mineralization

The bioweathering of REE minerals occurs at a scale that is of commercial value. In addition to their role in releasing REE through the weathering of minerals including monazite, fungi and bacteria can then concentrate the REE and are implicated in the formation of so-called regolith-hosted REE deposits [69].

Fluorocarbonates are more amenable to the extraction of REEs than oxide/phosphate minerals. Accordingly, research has been directed to model the hydrothermal evolution of REE phases to precipitate fluorocarbonates [70] and to patent a commercial laboratory version of the process [71]. The occurrence at Rhynie indicates that biological activity can contribute to this kind of transformation of REE in monazite to form desirable fluorocarbonates.

The biomarker perylene, which signifies fungal activity, is present in several shale samples in the studied section. The perylene is unlikely to have formed in the shale but rather has been washed into the lake from the adjacent land surface. The transport of perylene into water bodies is demonstrable today and is also recorded in other Devonian shales [72]. Land plants preserved in chert beds at Rhynie show extensive fungal colonization [19–21], so the transfer of perylene to the lake waters could have occurred readily. Samples of plant fossils on the adjacent land surface contain fossilized fungi in borehole 19C, including at the depths where fluorapatite mineralization occurs [73]. The evidence of fungal activity supports the model of biological alteration of monazite implied by its exceptional occurrence in the Rhynie chert succession.

4.6. Organic-Rich Sediments

In other cases where fluorocarbonates occur in shales, pelites, and coal, metamorphism was critical to mineralization. Metamorphism could have concentrated REEs from the organic-rich sediment. Most notably, the Columbian emerald deposits, which include gem-quality fluorocarbonates, are in metamorphosed black shales [41]. However, the Rhynie shales are not metamorphosed. The role of the shale at Rhynie was instead the occurrence of carbonate, which created the necessary alkaline environment.

Carbonates are common in organic-rich sediments in lacustrine environments, relative to open marine environments [74,75]. The lacustrine carbonates form during early diagenesis at shallow burial depths. The lacustrine shales are therefore a good focus for fluorocarbonate mineralization in continental sequences. As discussed above, ephemeral lakes that precipitate calcite and pyrite have Eh–pH conditions which are suitable for fluorocarbonate minerals.

5. Conclusions

Fluorocarbonate mineralization occurs in Lower Devonian carbonate-bearing shale within the Rhynie chert. The chert occurrence is spatially related to a granite outcrop. In most cases, the mineral phase has a composition referrable to synchysite. Unlike most examples of fluorocarbonate mineralization elsewhere, the occurrence in the Rhynie chert formed at a relatively low temperature. The mineralization was engendered by:

(i) Availability of REEs by bioweathering of monazite grains in the sequence, derived from underlying granite.

(ii) Availability of fluorine, evident as fluorite, associated with hot spring activity also related to underlying granite.

(iii) Precipitation in the alkaline environment of carbonate-bearing shales.

The rocks achieved a maximum burial temperature of about 110 °C but mineralization probably occurred at a lower temperature during shallow burial. This study supports a model for fluorocarbonate mineralization at relatively low temperatures and hence encourages the exploration for fluorocarbonate resources in rocks without a history of high temperatures.

References

1. Smith, M.P.; Henderson, P.; Peishan, Z. Reaction relationships in the Bayan obo Fe–REE–Nb deposit Inner Mongolia, China, implications for the relative stability of rare-earth element phosphates and fluorocarbonates. *Contrib. Mineral. Petrol.* **1999**, *134*, 294–310. [CrossRef]

2. Louvel, M.; Etschmann, B.; Guan, Q.; Testemale, D.; Brugger, J. Carbonate complexation enhances hydrothermal transport of rare earth elements in alkaline fluids. *Nat. Commun.* **2022**, *13*, 1456. [CrossRef]

3. Marien, C.; Dijkstra, A.; Wilkins, C. The hydrothermal alteration of carbonatite in the Fen Complex, Norway: Mineralogy, geochemistry, and implications for rare-earth element resource formation. *Mineral. Mag.* **2018**, *82*, S115–S131. [CrossRef]

4. Balaram, V. Rare earth elements: A review of applications, occurrence, exploration, analysis, recycling, and environmental impact. *Geosci. Front.* **2019**, *10*, 1285–1303. [CrossRef]

5. Benaouda, R.; Devey, C.W.; Badra, L.; Ennaciri, A. Light rare-earth element mineralization in hydrothermal veins related to the Jbel Boho alkaline igneous complex, AntiAtlas/Morocco: The role of fluid-carbonate interactions in the deposition of synchysite-(Ce). *J. Geochem. Explor.* **2017**, *177*, 28–44. [CrossRef]

6. Manfredi, T.R.; Bastos Neto, A.C.; Pereira, V.P.; Barbanson, L.; Schuck, C. The parisite-(Ce) mineralization associated with the Fazenda Varela carbonatite (Correia Pinto, SC). *Pesquisas em Geociências* **2013**, *40*, 295–307. [CrossRef]

7. Liu, Y.; Chen, Z.; Yang, Z.; Sun, X.; Zhu, Z.; Zhang, Q. Mineralogical and geochemical studies of brecciated ores in the Dalucao REE deposit, Sichuan Province, southwestern China. *Ore Geol. Rev.* **2015**, *70*, 613–636. [CrossRef]

8. Andersen, A.K.; Clark, J.G.; Larson, P.B.; Donovan, J.J. REE fractionation, mineral speciation, and supergene enrichment of the Bear Lodge carbonatites, Wyoming, USA. *Ore Geol. Rev.* **2017**, *89*, 780–807. [CrossRef]

9. Hoshino, M.; Watanabe, Y.; Murakami, H.; Kon, Y.; Tsunematsu, M. Formation process of zircon associated with REE-fluorocarbonate and niobium minerals in the Nechalacho REE deposit, Thor Lake, Canada. *Resour. Geol.* **2012**, *63*, 1–26. [CrossRef]

10. Pham-Ngoc, C.; Ishiyama, D.; Tran, T.A.; Hoshino, M.; Taguchi, S. Characteristic features of REE and Pb–Zn–Ag mineralizations in the Na Son Deposit, Northeastern Vietnam. *Resour. Geol.* **2016**, *66*, 404–418. [CrossRef]

11. Schmandt, D.S.; Cook, N.J.; Ciobanu, C.L.; Ehrig, K.; Wade, B.P.; Gilbert, S.; Kamenetsky, V.S. Rare Earth Element Fluorocarbonate Minerals from the Olympic Dam Cu-U-Au-Ag Deposit, South Australia. *Minerals* **2017**, *7*, 202. [CrossRef]

12. Majka, J.; Włodek, A.; Jonsson, E.; Högdahl, K. Contrasting coronas: Microscale fluid variation deduced from monazite breakdown products in altered metavolcanic rocks associated with the Grängesberg apatite-iron oxide ore, Bergslagen, Sweden. *GFF* **2022**, *144*, 89–96. [CrossRef]

13. Doroshkevich, A.G.; Viladkar, S.G.; Ripp, G.S.; Burtseva, M.V. Hydrothermal REE mineralization in the Amba Dongar carbonatite complex, Gujurat, India. *Can. Mineral.* **2009**, *47*, 1105–1116. [CrossRef]

14. Ishihara, S.; Hua, R.; Hoshino, M.; Murakami, H. REE abundance and REE minerals in granitic rocks in the Nanling Range, Jiangxi Province, southern China, and generation of the REE-rich weathered crust deposits. *Resour. Geol.* **2008**, *58*, 355–372. [CrossRef]

15. Rice, C.M.; Ashcroft, W.A.; Batten, D.J.; Boyce, A.J.; Caulfield, J.B.D.; Fallick, A.E.; Hole, M.J.; Jones, E.; Pearson, M.J.; Rogers, G.; et al. A Devonian auriferous hot spring system, Rhynie, Scotland. *J. Geol. Soc. Lond.* **1995**, *152*, 229–250. [CrossRef]

16. Rice, C.M.; Trewin, N.H.; Anderson, L.I. Geological setting of the Early Devonian Rhynie cherts, Aberdeenshire, Scotland: An early terrestrial hot spring system. *J. Geol. Soc. Lond.* **2002**, *159*, 203–214. [CrossRef]

17. Trewin, N.H.; Wilson, E. Correlation of the Early Devonian Rhynie chert beds between three boreholes at Rhynie, Aberdeenshire. *Scott. J. Geol.* **2004**, *40*, 73–81. [CrossRef]

18. Baron, M.; Hillier, S.; Rice, C.M.; Czapnik, K.; Parnell, J. Fluids and hydrothermal alteration assemblages in a Devonian gold-bearing hot-spring system, Rhynie, Scotland. *Trans. R. Soc. Edinb. Earth Sci.* **2004**, *94*, 309–324. [CrossRef]

19. Taylor, T.N.; Klavins, S.D.; Krings, M.; Taylor, E.L.; Kerp, H.; Hass, H. Fungi from the Rhynie Chert: A view from the dark side. *Trans. R. Soc. Edinb. Earth Sci.* **2004**, *94*, 457–473. [CrossRef]
20. Strullu-Derrien, C.; Kenrick, P.; Pressel, S.; Duckett, J.G.; Rioult, J.-P.; Strullu, D.-G. Fungal associations in Horneophyton ligneri from the Rhynie Chert (c. 407 million year old) closely resemble those in extant lower land plants: Novel insights into ancestral plant–fungus symbioses. *New Phytol.* **2014**, *203*, 964–979. [CrossRef]
21. Krings, M.; Harper, C.J.; Taylor, E.L. Fungi and fungal interactions in the Rhynie chert: A review of the evidence, with the description of *Perexiflasca tayloriana* gen. et sp. nov. *Philos. Trans. R. Soc. B* **2018**, *373*, 20160500. [CrossRef] [PubMed]
22. Keekan, K.K.; Jalondhara, J.C. *Aspergillus niger* PSSG8 mediated bioleaching of monazite for the recovery of rare earth and other metal constituents. *Adv. Mater. Res.* **2015**, *1130*, 238–242. [CrossRef]
23. Brisson, V.L.; Zhuang, W.Q.; Alvarez-Cohen, L. Bioleaching of rare earth elements from monazite sand. *Biotechnol. Bioeng.* **2016**, *113*, 339–348. [CrossRef] [PubMed]
24. Corbett, M.K.; Eksteen, J.J.; Niu, X.-Z.; Croue, J.-P.; Watkin, E.L. Interactions of phosphate solubilising microorganisms with natural rare-earth phosphate minerals: A study utilizing Western Australian monazite. *Bioprocess Biosyst. Eng.* **2017**, *40*, 929–942. [CrossRef] [PubMed]
25. Fathollahzadeh, H.; Eksteen, J.J.; Kaksonen, A.H.; Watkin, E.L.J. Role of microorganisms in bioleaching of rare earth elements from primary and secondary resources. *Appl. Microbiol. Biotechnol.* **2019**, *103*, 1043–1057. [CrossRef]
26. Castro, L.; Blázquez, M.L.; González, F.; Muñoz, J.A. Bioleaching of phosphate minerals using *Aspergillus niger*: Recovery of copper and rare earth elements. *Metals* **2020**, *10*, 978. [CrossRef]
27. Kang, X.; Csetenyi, L.; Gadd, G.M. Colonization and bioweathering of monazite by *Aspergillus niger*: Solubilization and precipitation of rare earth elements. *Environ. Microbiol.* **2021**, *23*, 3970–3986. [CrossRef]
28. Trewin, N.H.; Fayers, S.R. Macro to micro aspects of the plant preservation in the Early Devonian Rhynie cherts, Aberdeenshire, Scotland. *Earth Environ. Sci. Trans. R. Soc. Edinb.* **2015**, *106*, 67–80. [CrossRef]
29. Marynowski, L.; Smolarek, J.; Bechtel, A.; Phillippe, M.; Kurkiewicz, S.; Simoneit, B.R.T. Perylene as an indicator of conifer fossil wood degradation by wood-degrading fungi. *Org. Geochem.* **2013**, *59*, 143–151. [CrossRef]
30. Schito, A.; Romano, C.; Corrado, S.; Grigo, D.; Poe, B. Diagenetic thermal evolution of organic matter by Raman spectroscopy. *Org. Geochem.* **2017**, *106*, 57–67. [CrossRef]
31. Schito, A.; Corrado, S. An automatic approach for characterization of the thermal maturity of dispersed organic matter Raman spectra at low diagenetic stages. *Geol. Soc. Lond. Spec. Publ.* **2020**, *484*, 107–119. [CrossRef]
32. Barker, C.E.; Pawlewicz, M.J. The correlation of vitrinite reflectance with maximum temperature in humic organic matter. In *Paleogeothermics*; Lecture Notes in Earth Sciences; Buntebarth, G., Stegena, L., Eds.; Springer: Berlin/Heidelberg, Germany, 1986; Volume 5, pp. 79–93.
33. Szakáll, S.; Nagy, G.; Sajó, I.E. Synchysite-(Ce) from the Komló coal deposit, Mecsek Mts., South Hungary. *Acta Mineral.-Petrogr. Abstr. Ser.* **2003**, *1*, 100.
34. Capitani, G. Synchysite-(Ce) from Cinquevalli (Trento, Italy): Stacking disorder and the polytypism of (Ca,REE)-Fluorcarbonates. *Minerals* **2020**, *10*, 77. [CrossRef]
35. Janots, E.; Negro, F.; Brunet, F.; Goffé, B.; Engi, M.; Bouybaouène, M.L. Evolution of the REE mineralogy in HP-LT metapelites of the Sebtide complex, Rif, Morocco: Monazite stability and geochronology. *Lithos* **2006**, *87*, 214–234. [CrossRef]
36. Förster, H.J. Synchysite-(Y)-synchysite-(Ce) solid solutions from Markersbach, Erzgebirge, Germany: REE and Th mobility during high-T alteration of highly fractionated aluminous A-type granites. *Mineral. Petrol.* **2001**, *72*, 259–280. [CrossRef]
37. Kříbek, B.; Knésl, I.; Dobeš, P.; Veselovský, F.; Pořádek, P.; Škoda, R.; Čopjaková, R.; Leichmann, J.; Košek, F. The origin of synchysite-(Ce) and sources of rare-earth elements in the Rožná uranium deposit, Czech Republic. *Minerals* **2022**, *12*, 690. [CrossRef]
38. Smith, M.; Kynicky, J.; Xu, C.; Song, W.; Spratt, J.; Jeffries, T.; Brtnicky, M.; Kopriva, A.; Cangelosi, D. The origin of secondary heavy rare earth element enrichment in carbonatites: Constraints from the evolution of the Huanglongpu district, China. *Lithos* **2018**, *308–309*, 65–82. [CrossRef]
39. Ayupova, N.; Melekestseva, I.; Maslennikov, V.; Sadykov, S. Mineralogy and geochemistry of clastic sulfide ores from the Talgan VHMS deposit, South Urals, Russia: Signatures of diagnostic alteration. *Ore Geol. Rev.* **2022**, *144*, 104839. [CrossRef]
40. Bucher, K.; Seelig, U. Bristen granite: A highly differentiated, fluorite-bearing A-type granite from the Aar massif, Central Alps, Switzerland. *Swiss J. Geosci.* **2018**, *111*, 317–340. [CrossRef]
41. Zeug, M.; Nasdala, L.; Ende, M.; Habler, G.; Hauzenberger, C.; Chanmaung, C.; Škoda, R.; Topa, D.; Wildner, M.; Wirth, R. The parisite-(Ce) enigma: Challenges in the identification of fluorcarbonate minerals. *Mineral. Petrol.* **2021**, *115*, 1–19. [CrossRef]
42. Trabucho-Alexandre, J. More gaps than shale: Erosion of mud and its effect on preserved geochemical and palaeobiological signals. *Geol. Soc. Lond. Spec. Publ.* **2014**, *404*, 251–270. [CrossRef]
43. Parviainena, A.; Loukola-Ruskeeniemi, K. Environmental impact of mineralised black shales. *Earth-Sci. Rev.* **2019**, *192*, 65–90. [CrossRef]
44. Bishop, B.A.; Shivakumar, K.R.; Alessi, D.S.; Robbins, L.J. Insights into the rare earth element potential of coal combustion by-products from western Canada. *Environ. Sci. Adv.* **2023**, *2*, 529–542. [CrossRef]
45. Wang, Q.; Morse, J.W. Pyrite formation under conditions approximating those in anoxic sediments I. Pathway and morphology. *Mar. Chem.* **1996**, *2*, 99–121. [CrossRef]

46. Lottermoser, B.G.; Cleverley, J.S. Controls on the genesis of a high-fluoride thermal spring: Innot Hot Springs, north Queensland. *Aust. J. Earth Sci.* **2007**, *54*, 597–607. [CrossRef]

47. Shitumbanuma, V.; Tembo, F.; Tembo, J.M.; Chilala, S.; Van Ranst, E. Dental fluorosis associated with drinking water from hot springs in Choma district in southern province, Zambia. *Environ. Geochem. Health* **2007**, *29*, 51–58. [CrossRef]

48. Addison, M.J.; Rivett, M.O.; Phiri, O.L.; Milne, N.; Milne, V.; McMahon, A.D.; Macpherson, L.M.D.; Bagg, J.; Conway, D.I.; Phiri, P.; et al. 'Hidden Hot Springs' as a source of groundwater fluoride and severe dental fluorosis in Malawi. *Water* **2021**, *13*, 1106. [CrossRef]

49. Chesworth, W.; Martínez Cortizas, A.; García-Rodeja, E. The redox–pH approach to the geochemistry of the Earth's land surface, with application to peatlands. In *Peatlands: Evolution and Records of Environmental and Climate Changes*; Martini, I.P., Martínez Cortizas, A., Chesworth, W., Eds.; Elsevier: Amsterdam, The Netherlands, 2006; pp. 175–195.

50. Liu, X.; Wang, Q.; Zhang, Q.; Zhang, Y.; Li, Y. Genesis of REE minerals in the karstic bauxite in western Guangxi, China, and its constraints on the deposit formation conditions. *Ore Geol. Rev.* **2016**, *75*, 100–115. [CrossRef]

51. Mackie, W. The heavier accessory minerals in the granites of Scotland. *Trans. Edinb. Geol. Soc.* **1925**, *12*, 22–40. [CrossRef]

52. Plant, J.A.; Henney, P.J.; Simpson, P.R. The genesis of tin-uranium granites in the Scottish Caledonides: Implications for metallogenesis. *Geol. J.* **1990**, *25*, 431–442. [CrossRef]

53. Ansberque, C.; Mark, C.; Caulfield, J.T.; Chew, D.M. Combined in-situ determination of halogen (F, Cl) content in igneous and detrital apatite by SEM-EDS and LA-Q-ICPMS: A potential new provenance tool. *Chem. Geol.* **2019**, *524*, 406–420. [CrossRef]

54. Tindle, A.G.; Webb, P.C. Estimation of lithium contents in trioctahedral micas using microprobe data: Application to micas from granitic rocks. *Eur. J. Mineral.* **1990**, *2*, 595–610. [CrossRef]

55. Gould, D. *Geology of the Aboyne District. Memoir of the British Geological Survey, Sheet 66W (Scotland)*; The Stationery Office: London, UK, 2001.

56. Smith, C.G.; Goodman, S.; Robertson, S. *Geology of the Ballater District. Memoir of the British Geological Survey, Sheet 65E (Scotland)*; The Stationery Office: London, UK, 2002.

57. Oliver, G.J.H.; Wilde, S.A.; Wan, Y. Geochronology and geodynamics of Scottish granitoids from the late Neoproterozoic break-up of Rodinia to Palaeozoic collision. *J. Geol. Soc. Lond.* **2008**, *165*, 661–674. [CrossRef]

58. Mark, D.F.; Rice, C.M.; Fallick, A.E.; Trewin, N.H.; Lee, M.R.; Boyce, A.; Lee, J.K.W. 40Ar/39Ar dating of hydrothermal activity, biota and gold mineralization in the Rhynie hot-spring system, Aberdeenshire, Scotland. *Geochim. Cosmochimca Acta* **2011**, *75*, 555–569. [CrossRef]

59. Hall, A.; Walsh, J.N. Zinnwaldite granite from Glen Gairn, Aberdeenshire. *Scott. J. Geol.* **1972**, *8*, 265–267. [CrossRef]

60. Webb, P.C.; Tindle, A.G.; Ixer, R.A. W-Sn-Mo-Bi-Ag mineralization associated with zinnwaldite-bearing granite from Glen Gairn, Scotland. *Trans. Inst. Min. Metall. (Sect. B Appl. Earth Sci.)* **1992**, *101*, B59–B72.

61. Parnell, J.; Akinsanpe, T.O.; Armstrong, J.G.; Boyce, A.J.; Still, J.W.; Bowden, S.A.; Clases, D.; Gonzalez de Vega, R.; Feldmann, J. Trace element geochemistry in the earliest terrestrial ecosystem, the Rhynie Chert. *Geochem. Geophys. Geosyst.* **2022**, *23*, e2022GC010647. [CrossRef]

62. Colman, T.B.; Beer, K.E.; Cameron, D.G.; Kimbell, G.S. *Molybdenum Mineralisation near Chapel of Garioch, Inverurie, Aberdeenshire*; British Geological Survey Technical Report WF/89/3, Mineral Reconnaissance Programme Report 100; British Geological Survey: Keyworth, UK, 1989.

63. Zhu, X.K.; O'Nions, R.K. Monazite chemical composition: Some implications for monazite geochronology. *Contrib. Mineral. Petrol.* **1999**, *137*, 351–363. [CrossRef]

64. Bern, C.R.; Shah, A.K.; Benzel, W.M.; Lowers, H.A. The distribution and composition of REE-bearing minerals in placers of the Atlantic and Gulf coastal plains, USA. *J. Geochem. Explor.* **2016**, *162*, 50–61. [CrossRef]

65. Ciobanu, C.L.; Cook, N.J.; Slattery, A.D.; Ehrig, K.; Liu, W.Y. Nanoscale intergrowths in the bastnäsite–synchysite series record transition toward thermodynamic equilibrium. *MRS Bull.* **2022**, *47*, 250–257. [CrossRef]

66. Ciobanu, C.L.; Kontonikas-Charos, A.; Slattery, A.; Cook, N.J.; Ehrig, K.; Wade, B.P. Short-range stacking disorder in mixed-layer compounds: A HAADF STEM study of bastnäsite-parisite intergrowths. *Minerals* **2017**, *7*, 227. [CrossRef]

67. Fame, M.L.; Spotila, J.A.; Owen, L.A.; Dortch, J.N.; Shuster, D.L. Spatially heterogeneous post-Caledonian burial and exhumation across the Scottish Highlands. *Lithosphere* **2018**, *10*, 406–425. [CrossRef]

68. Wellman, C.H. Palaeoecology and palaeophytogeography of the Rhynie chert plants: Evidence from integrated analysis of in situ and dispersed spores. *Proc. R. Soc. Biol. Sci.* **2004**, *271*, 985–992. [CrossRef] [PubMed]

69. Li, X.; Liang, X.; He, H.; Li, J.; Ma, L.; Tan, W.; Zhong, Y.; Zhu, J.; Zhou, M.; Song, H. Microorganisms accelerate REE mineralization in supergene environments. *Appl. Environ. Microbiol.* **2022**, *88*, e00632-22. [CrossRef]

70. Strzelecki, A.C.; Migdisov, A.; Boukhalfa, H.; Sauer, K.; McIntosh, K.G.; Currier, R.P.; Williams-Jones, A.E.; Guo, X. Fluocerite as a precursor to rare earth element fractionation in ore-forming systems. *Nat. Geosci.* **2022**, *15*, 327–333. [CrossRef]

71. Fernando, Q.; Yanagihara, N.; Dyke, J.T.; Vemulapalli, K. Formation of Rare Earth Carbonates Using Supercritical Carbon Dioxide. U.S. Patent 5045289, 3 September 1991.

72. Philp, R.P.; De Garmo, D. Geochemical characterization of the Devonian-Mississippian Woodford Shale from the McAlister Cemetery Quarry, Criner Hills Uplift, Ardmore Basin, Oklahoma. *Mar. Pet. Geol.* **2020**, *112*, 104078. [CrossRef]

73. Powell, C.L.; Trewin, N.H.; Edwards, D. Palaeoecology and plant succession in a borehole through the Rhynie cherts, Lower Old Red Sandstone, Scotland. *Geol. Soc. Lond. Spec. Publ.* **2000**, *180*, 439–457. [CrossRef]

74. Dean, W.E. The carbon cycle and biogeochemical dynamics in lake sediments. *J. Paleolimnol.* **1999**, *21*, 375–393. [CrossRef]
75. Gierlowski-Kordesch, E.H. Lacustrine carbonates. *Dev. Sedimentol.* **2010**, *61*, 1–101.